Bioconjugate Chemistry

Article

Cite This: *Bioconjugate Chem.* 2018, 29, 126−135

pubs.acs.org/bc

Self-Transfecting Micellar RNA: Modulating Nanoparticle Cell Interactions via High Density Display of Small Molecule Ligands on Micelle Coronas

Alexander Roloff,[†] David A. Nelles,[§,⊥] Matthew P. Thompson,[†] Gene W. Yeo,[*,‡,§] and Nathan C. Gianneschi[*,†,⊥,¶]

[†]Department of Chemistry & Biochemistry, [‡]Stem Cell Program and Institute for Genomic Medicine, [§]Department of Cellular and Molecular Medicine, and [⊥]Materials Science and Engineering, University of California, San Diego, La Jolla, California 92093, United States

[¶]Department of Chemistry, Materials Science and Engineering, Biomedical Engineering, Northwestern University, Evanston, Illinois 60208, United States

Supporting Information

ABSTRACT: The intracellular delivery of synthetic nucleic acids represents a major challenge in biotechnology and in biomedicine. Methods to deliver short, double-stranded RNA to living cells are of particular interest because of the potential to engage the RNA interference machinery and to regulate *m*RNA expression. In this work, we describe novel RNA-polymer amphiphiles that assemble into spherical micellar nanoparticles with diameters of ca. 15−30 nm and efficiently enter live cells without transfection reagents. Each micelle consists of approximately 100 RNA strands forming a densely packed corona around a polymeric core. Importantly, the surface-displayed RNA remains accessible for hybridization with complementary RNA. Chemical modification of the termini of hybridized RNA strands enabled the display of small organic moieties on the outer surface of the micelle corona. We found that some of these modifications can have a tremendous impact on cellular internalization efficiencies. The display of hydrophobic dabcyl or stilbene units dramatically increased cell uptake, whereas hydrophilic neutral hydroxy or anionic phosphate residues were ineffective. Interestingly, neither of these modifications mediated noticeable uptake of free RNA oligonucleotides. We infer that their high density display on micellar nanoparticle surfaces is key for the observed effect; achieved with local effective surface concentrations in the millimolar range. We speculate that weak interactions with cell surface receptors that are amplified by the multivalent presentation of such modifications may be responsible. The installation of small molecule ligands on nanomaterial surfaces via hybridization of chemically modified oligonucleotides offers a simple and straightforward way to modulate cellular uptake of nanoparticles. Biological functionality of micellar RNA was demonstrated through the sequence-specific regulation of *m*RNA expression in HeLa cells.

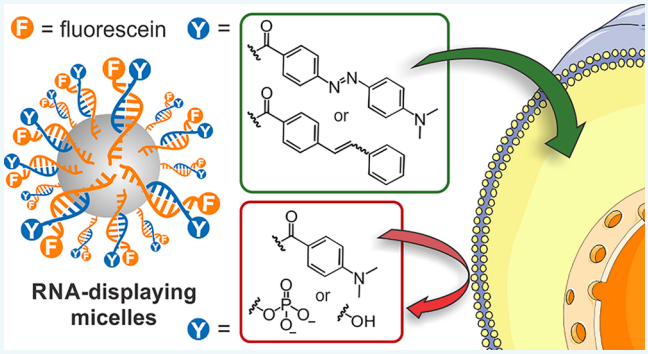

INTRODUCTION

As the primary means of information storage and transfer in living systems, nucleic acids have gained considerable attention as powerful tools in biomedicine.[1−4] In particular, RNA is known to form a diverse set of bioactive species including aptamers,[5] ribozymes,[6] microRNAs,[7] and short interfering RNAs[8] (siRNAs) that can effectively modulate cell behavior. Despite their success, the implementation of small RNAs in relevant biological settings has been hindered by difficulties including stability and delivery. The high negative charge of nucleic acids, especially in the duplex form, severely impedes the penetration of lipid bilayer cell membranes. Virus-based strategies to transfect nucleic acids into cells bear the risk of triggering dangerous immune responses.[9,10] Alternatively, cationic lipo- and polyplex-based transfection reagents are popularly utilized to complex the polyanionic oligonucleotides, neutralizing their charge and thereby facilitating transport.[11−15] Unfortunately, many of these formulations operate via mechanisms that are toxic to cells.[16] Their multicomponent nature can leave unassociated polycationic material behind that may associate with the cell membrane and interfere with biological processes.

Recently, RNA has been established as a building block for the preparation of nanomaterials.[17−19] For example, the high density display of RNA on gold nanoparticle surfaces mediates cell uptake of the resulting spherical nucleic acids (SNAs).[20−23]

Received: October 27, 2017
Revised: November 22, 2017
Published: December 29, 2017

DOI: 10.1021/acs.bioconjchem.7b00657
Bioconjugate Chem. 2018, 29, 126−135

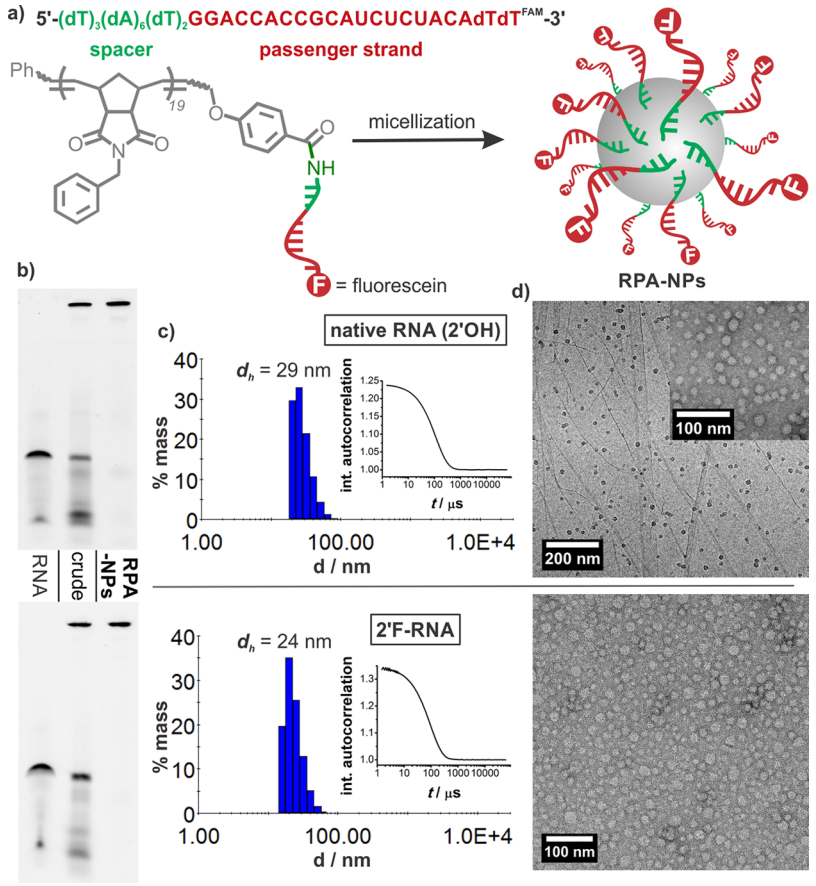

Figure 1. (a) Nucleic acid sequence and polymer structure of RNA-polymer amphiphiles (RPAs) that assemble into micellar **RPA-NPs**. Nanoparticles displaying native and 2′-fluoro-pyrimidine-modified passenger RNAs were characterized via (b) PAGE (before and after SEC purification), (c) DLS (autocorrelation functions are shown in insets), and (d) TEM (unstained on graphene oxide (top) and stained on carbon/Formvar-coated copper (top insert + bottom). See Figures S2−S4 for additional characterization.

SNAs have served to overcome many barriers associated with popular delivery techniques. While very successful in recent applications,[24,25] the chemical functionality in these systems is limited by virtue of the metal scaffolding and templating approach. Furthermore, accumulation-induced toxicity of gold nanoparticles can be an issue.[26−28]

We recently demonstrated that amphiphilic conjugates of DNA and hydrophobic polymers assemble into micellar nanoparticles.[29−32] These DNA-displaying micelles efficiently internalize into different cell lines without the need for toxic transfection reagents. Furthermore, regulation of intracellular *m*RNA levels was accomplished when antisense DNA/LNA chimeras were incorporated into the sequence.[33] However, antisense-based approaches cannot engage the highly efficient RNA interference (RNAi) machinery of the cell. Hence, we set out to develop novel RNA−polymer amphiphiles (RPAs) that would assemble into micellar nanoparticles (**RPA-NPs**) displaying RNA at high density on the surface of a soft organic polymeric core. These quasi-single component systems can hybridize with complementary RNA, generating double-stranded biologically active micellar siRNA. We found that chemical modifications of the hybridized RNA strands dramatically influence the cell uptake efficiency of **RPA-NPs**, depending on the nature of the chemical moiety that is displayed at high effective concentration on the micelle corona. Internalization efficiencies correlated with knockdown potentials toward the target *survivin* *m*RNA in HeLa cells. We believe that the high density display of chemically modified nucleic acids via hybridization into the coronas of nucleic acid-displaying nanomaterials offers a simple and straightforward way to modulate cellular uptake.

RESULTS

Assembling Micellar RNA from RNA-Polymer Amphiphiles. We designed RNA-polymer amphiphiles that would assemble into micellar nanoparticles (**RPA-NPs**) in aqueous solution driven by hydrophobic interactions of the polymer chains. The packing of the polymeric core aligns the conjugated RNA strands at high density within the micelle corona. We chose an RNA sequence that encodes the passenger strand of a 21 base pair siRNA duplex directed against the *survivin* *m*RNA,[34−36] whose overexpression is associated with cancer.

The synthesis of **RPA-NPs** was derived from a previously established route for DNA-polymer amphiphile nanoparticles.[31−33] Briefly, a solid support-bound fully protected oligonucleotide that was equipped with an amino group on its 5′-terminus was conjugated to a carboxy-terminated hydrophobic polymer of (*N*-benzyl)-5-norbornene-exo-2,3-dicarboximide with an average chain length of 19, that was synthesized via ring-opening metathesis polymerization (see Figure S1 in the Supporting Information for details). Extensive washing after the coupling reaction ensured that no unreacted polymer can integrate into the micelle core, providing for exceptionally dense nucleic acid packing in the corona. We

DOI: 10.1021/acs.bioconjchem.7b00657
Bioconjugate Chem. 2018, 29, 126−135

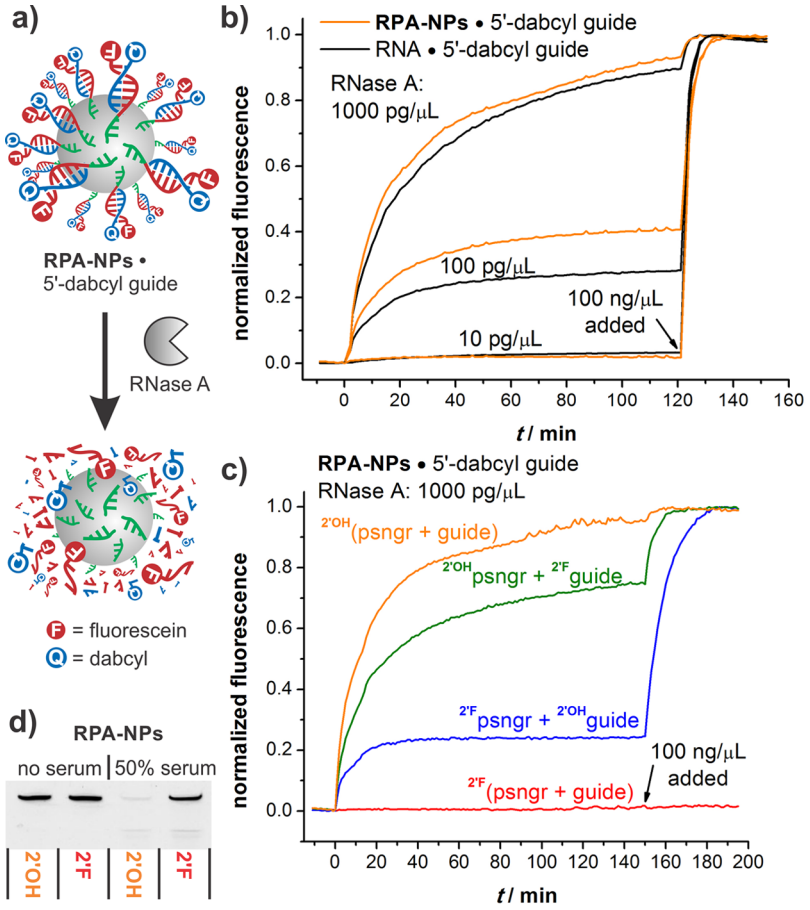

Figure 2. (a) Cleavage of **RPA-NP** duplexes by RNase A separates the fluorescein dye from the dabcyl quencher, leading to an increase in fluorescence intensity. (b) Comparison of processing rates of micellar and free RNA duplexes. (c) Processing rates of native 2′OH-RNA and 2′F-RNA in **RPA-NP** duplexes. (d) PAGE analysis of **RPA-NPs** and **2′F-RPA-NPs** after incubation in human serum for 97 h (also see Figure S7a).

included an 11-mer DNA spacer[33,37] between the RNA sequence and the polymer attachment site in order to provide space within the micelle corona for hybridization with the complementary guide RNA. Furthermore, a fluorescein label was incorporated on the outermost deoxythymidine (dT) nucleotide at the 3′-terminus of the sequence to facilitate particle tracking in cell uptake studies.

After cleavage from the support and deprotection, RPAs spontaneously assembled into spherical micellar **RPA-NPs** (Figure 1a). The micelles were separated from any unconjugated RNA via size exclusion chromatography (SEC), and purity was verified by poly(acrylamide) gel electrophoresis (PAGE, Figure 1b). Dynamic light scattering (DLS) experiments revealed a narrow size distribution, with most micelles having hydrodynamic diameters between 15 and 30 nm (Figure 1c). Transmission electron microscopy (TEM) imaging indicated the presence of spherical nanoparticles with similar diameters in the dry state (Figure 1d). The high glass transition temperature of the polymer, which is above the boiling point of water,[38] facilitates kinetic trapping of the nanoparticles and stabilizes them against disruption into amphiphiles.

Since results from gold-based SNAs indicated that degradation of surface-displayed RNA by serum nucleases can occur rapidly in certain sequence contexts,[22,39,40] we also synthesized **2′F-RPA-NPs** that incorporate 2′-fluoropyrimidines within the RNA sequence. This sugar modification has proven useful in mediating nuclease resistance and reducing immunogenicity while maintaining efficacy of siRNAs.[41−43] Static light scattering experiments revealed that each micelle displayed approximately 100−120 nucleic acid strands, which translates into exceptionally high effective RNA concentrations on the nanoparticle surface in the order of 20−90 mM (Table S1). Of note, the synthesis of this new class of RNA-based nanomaterial was reproducibly achieved with very little batch-to-batch and sequence-to-sequence variation (Figures S2−S4).

The formation of double-stranded **RPA-NPs** is a necessity for the generation of biologically active siRNA-displaying micelles. Once inside the cell, the hybridized guide RNA can bind to complementary *m*RNA targets and induce their degradation via the RNAi pathway.[44] Melting and fluorescence studies with a 5′-quencher-labeled guide RNA indicated that the surface-displayed RNA in both **RPA-NPs** and **2′F-RPA-NPs** remains accessible for hybridization with complementary RNA (Figure S5). The hydrodynamic diameter was not significantly changed upon hybridization (Figure S6).

Stability of Micellar RNA against Nucleolytic Degradation. The micellar RNA is exposed to a variety of nucleases present in the intracellular environment as well as in the serum that is commonly added to cell culture medium. We therefore investigated the susceptibility of **RPA-NPs** toward nucleolytic degradation in a real-time kinetic experiment. RNase A was chosen as a highly abundant serum endonuclease that cleaves after 3′-phosphates of pyrimidine nucleotides. **RPA-NPs** or corresponding free RNAs were hybridized with a 5′-dabcyl-labeled guide RNA. Hybridization was accompanied by quenching of the fluorescein dye in the outer corona of the

DOI: 10.1021/acs.bioconjchem.7b00657
Bioconjugate Chem. 2018, 29, 126−135

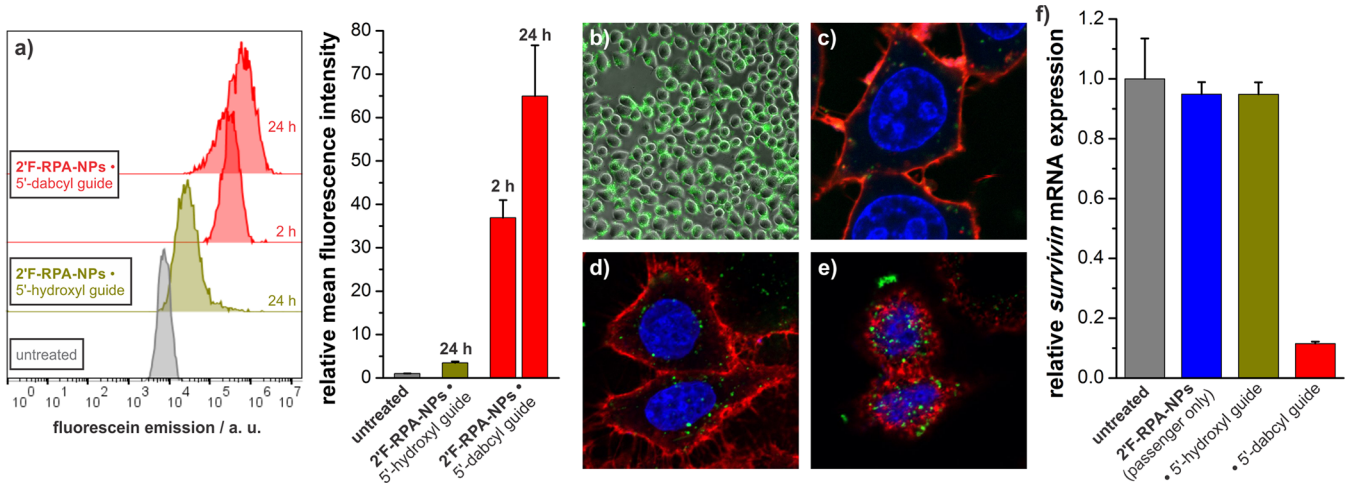

Figure 3. (a) Representative histograms and corresponding mean fluorescence intensities from flow cytometry measurements as well as (b) fluorescence and (c–e) confocal fluorescence microscopy images of HeLa cells treated with **2′F-RPA-NPs**·5′-dabcyl guide (green: fluorescein channel (**2′F-RPA-NPs**), blue: nucleus stain, red: membrane stain). Images of live cells are shown in (b) and (c). (d) and (e) depict images of two focal planes (cross section and top) of the same two fixed cells (see Figures S8–11 for additional images). (f) Relative *survivin* *m*RNA expression levels in HeLa cells treated with indicated micellar RNAs (3× 1 μM RNA (ca. 10 nM micelles) within 3 d in serum-free medium (see Supporting Information for detailed treatment protocols).

micelle or the free duplex (Figure S5). Nuclease-mediated cleavage of the phosphodiester linkages resulted in a fluorescence signal increase due to the separation of the chromophores upon dissociation of shorter fragments (Figure 2a). The similar kinetic profiles for the nucleolytic digestion reactions with micellar and free RNA duplexes at different RNase A concentrations suggested that both species are similarly accessible for the enzyme (Figure 2b). This stands in contrast to previously observed resistance of DNA-displaying micellar nanoparticles against degradation by certain DNases.[31,32,45] We assume that this lack of specificity toward the substrate duplex—either three-dimensionally arranged on a densely packed micelle corona or free in solution—originates in the relatively small size and very high catalytic activity of RNase A, whose processing rate is diffusion-controlled.[46,47] However, the 2′-fluoro modification of ribose provided a suitable means to render the nanoparticles inert against nucleolytic degradation. If a 2′-fluoropyrimidine-containing guide strand was incorporated in the micellar duplex, the rate of the cleavage reaction was moderately decreased (Figure 2c, green curve). When the same modification was included in the passenger strand, the effect was more pronounced, presumably due to the greater number of pyrimidines in its sequence (Figure 2c, blue curve). Finally, if both strands contained 2′-fluoropyrimidines, there was no detectable RNA cleavage over the course of the experiment (Figure 2c, red curve). Importantly, **2′F-RPA-NPs** were also stable in 50% human serum for at least 97 h (Figure 2d), and could be stored in solution at 10 °C for several months, without any significant release of amphiphiles (Figure S7b).

Cell Uptake and *m*RNA Regulation in HeLa Cells. We went on to study the uptake of stabilized fluorescein-labeled **2′F-RPA-NPs** in HeLa cells. We initially investigated two different micellar duplexes. The first included a guide RNA with a 5′-hydroxyl group on the terminal ribose. The guide strand of the second duplex carried a dabcyl label that was connected via an aminododecyl phosphodiester to the 5′-hydroxide, which we had on hand from nuclease resistance studies. To our surprise, flow cytometry experiments revealed a much higher increase of cell-associated fluorescence for cells treated with the micelles hybridized to the 5′-dabcyl-modified guide RNA (Figure 3a). In these studies, after only 2 h of incubation, the relative increase exceeded that of cells treated for 24 h with the 5′-hydroxylated micellar duplex by 10-fold. A 65-fold signal gain over background was observed after 24 h. Note that the 5′-dabcyl moiety quenches the fluorescein dye in the nanoparticle shell significantly (Figure S5e), such that these relative values are only semiquantitative and call for much greater differences in the actual uptake efficiencies (*vide infra*). As we gated for live cells in flow cytometry analyses, any signal must come from nanomaterial that is associated with the cells. Cleavage of RNA or micelle disruption prior to internalization (which we did not observe in serum stability studies in Figure 2) would lead to loss of dye and therefore not contribute to the measured signal.

Confocal fluorescence microscopy experiments revealed that the nanomaterial was internalized into cells, as evident from punctuate fluorescence appearing on the cytoplasmic side of the cell membrane (Figure 3b–e and Figure S8–S11, green channel). Some of the material also seemed to be associated with the cell membrane, possibly reflecting an earlier stage of the internalization process.

The cell uptake efficiencies correlated with the potential of the micellar siRNA duplexes to regulate *m*RNA expression (Figure 3f). Only the internalized micellar duplex containing the 5′-dabcyl-labeled guide RNA was capable of reducing *survivin* *m*RNA levels by 90%, which compares favorably to previous antisense DNA/LNA-derived micelles tested under similar conditions.[33] This efficacy in gene silencing also indicates that at least a portion of the nanomaterial accesses the cytosol where the *m*RNA target resides, and is not stuck in endosomal compartments. Micelles incorporating the 5′-hydroxylated guide were as inefficient as nanoparticles that were lacking a guide strand. It is worth mentioning that 5′-phosphates are preferable structural elements for efficient binding of guide RNAs to the RNA-induced silencing complex (RISC). However, it has been demonstrated previously that modifications can be tolerated if the guide strand maintains a 5′-phosphodiester structure.[48–50] Some of the 5′-modifications

DOI: 10.1021/acs.bioconjchem.7b00657
Bioconjugate Chem. 2018, 29, 126–135

might also be hydrolyzed by intracellular phosphodiesterases[51] providing active 5′-phosphorylated guides. It is also possible that alternative pathways such as translational repression or degradation of the *m*RNA by RNases that are not associated with the RISC play a role.

The *survivin* mRNA knockdown was dose-dependent, and still efficient if the micellar siRNA was directly added to the serum-containing cell culture medium, which highlights the stability of this RNA-based nanomaterial in a challenging biological environment (Figure 4a). We observed no

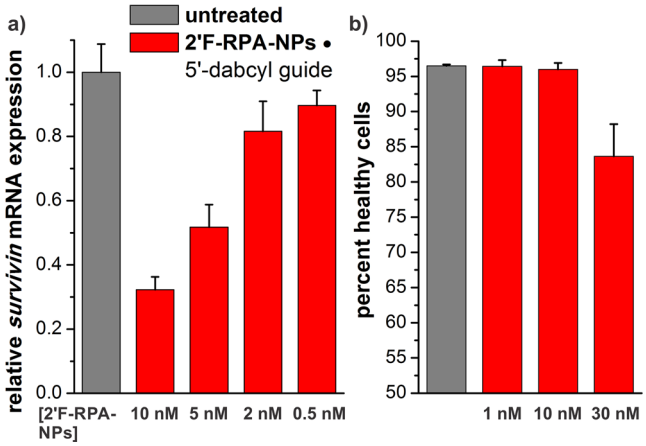

Figure 4. (a) Dose dependency of *survivin* *m*RNA knockdown in HeLa cells treated with micellar siRNA (single treatment in serum-containing medium, analyzed after 52 h). (b) Cytotoxicity in HeLa cells after treatment with different doses of micellar siRNA in serum-containing medium (analyzed after 28 h, see also Figure S12 and text for detailed treatment protocols).

cytotoxicity at relevant doses, as measured by a propidium iodide assay (Figure 4b), although some toxicity emerged at higher concentrations. Of note, we also observed toxicity when treating cells with a conventional cationic lipid-based transfection reagent at much lower RNA concentrations (Figure S12).

Influence of the Surface-Displayed Chemical Structure on Cell Uptake of Micellar RNA. It was evident from our initial uptake experiments (Figure 3a) that the high-density display of a dabcyl moiety on the micelle surface enhanced cellular recognition and uptake of micellar RNA. Therefore, we were curious as to the structural element responsible for this effect. Modifications can be readily installed on the micelle surface via hybridization with chemically functionalized guide RNAs. Hence, we synthesized guide strands bearing chemically similar but distinct 5′-modifications (Figure 5a). Specifically, 4-*N*,*N*-dimethylaminobenzoic acid (DMAB) resembles the *N*,*N*-dimethylamino-phenyl group of dabcyl but lacks the phenyl-azo portion, whereas 4-stilbene carboxylic acid resembles a similar conjugated π-system as dabcyl but incorporates a C═C instead of the N═N double bond and lacks the tertiary exocyclic amine. We also synthesized a 5′-phosphorylated guide RNA that is negatively charged at the terminus. Furthermore, to investigate the dependency of cell uptake on the sequence context as well as the selectivity of *m*RNA regulation, we synthesized **2′F-RPA-NPs** that display a nonsense RNA sequence, together with the corresponding guide RNAs without significant homology to any known human *m*RNA sequence. **2′F-RPA-NPs** of both sequences were comparable in size and morphology as well as nucleic acid surface density (Figure S4, Table S1), and hybridization of all 5′-modified guide RNAs to **2′F-RPA-NPs** was verified by melting experiments (Figure S5f). Fluorescence spectroscopy measurements indicated that the quenching efficiencies of DMAB and stilbene modifications were markedly reduced compared to the parent dabcyl structure (Figure 5b). The phosphorylated guide even enhanced emission compared to the single-stranded micelles, probably due to reduced self-quenching of the surface-displayed fluorescein dye in the fully stretched duplexes within the micelle corona (see Figure S5e and text for a detailed analysis).

Next, we performed cell uptake experiments with different combinations of **2′F-RPA-NPs** and guide RNAs. First, we compared the uptake of single- and double-stranded micelles with their corresponding free RNA duplexes bearing the same 5′-modifications on the guide strands (Figure 5c). Flow cytometry measurements revealed that the single-stranded micelles as well as the micellar duplex bearing a 5′-phosphate on the guide strand did not efficiently associate with cells, which verifies that the fluorescein dye alone does not mediate cellular uptake of the RNA-displaying nanomaterial. We note that this contrasts results from polymeric micelles displaying single-stranded DNA, which have been reported to efficiently internalize into HeLa cells.[33] We speculate that RNA strands adopt secondary structures within the micelle corona that are distinct from DNA, thus leading to different molecular surface structures unfavorable for cellular recognition. If a 5′-dabcylated guide RNA was incorporated in the micelle corona, a 70-fold fluorescence increase over background was measured after 24 h, which correlates well with our initial results (compare Figure 3a). A much higher 852-fold increase was observed for the stilbene-modified micellar duplex. This ca. 12-fold greater value lies within the range of the reduced quenching efficiency of stilbene compared to dabcyl (ca. 8-fold). Therefore, both the dabcyl- and stilbene-displaying micellar duplexes are presumably taken up with similar efficiencies. Contrarily, the DMAB-modified micellar duplex only triggered a 20-fold fluorescence increase (Figure 5d). Given the 3-fold brighter fluorescence of the DMAB-displaying duplex compared to its dabcyl-presenting counterpart, this modification is clearly less efficient in mediating nanoparticle uptake. Of note, none of the tested modifications are expected to be protonated at physiological pH, as the pK_as of dabcyl-related dyes such as methyl yellow/orange/red are within the range of 3.3−5.0. This indicates that the observed enhancement in cellular uptake does not rely on ionic interactions with the negatively charged cell membrane, as is the case for polycationic peptides and polymers. Importantly, at the same nucleic acid concentrations none of the free 2′F-RNA duplexes induced significant fluorescent signals in treated cells. Thus, it is indeed the high density display of the specific chemical moieties on the surface of the micellar nanoparticles that causes their association with and uptake into cells, and not the modification alone that is responsible.

We also compared **2′F-RPA-NPs** that resemble the *survivin* sequence with those incorporating a nonsense sequence (Figure 5d). Uptake efficiencies were similar for both nanomaterials and therefore independent of the sequence context (5′-dabcyl: 67- vs 83-fold, 5′-stilbene: 590- vs 804-fold for *survivin* and nonsense sequences, respectively) and also verified in HepG2 cells (Figure S13). However, only the *survivin* targeting **2′F-RPA-NPs** significantly reduced *m*RNA expression levels, which suggests a sequence-specific knockdown of the *mRNA* target (Figure 5e).

DOI: 10.1021/acs.bioconjchem.7b00657
Bioconjugate Chem. 2018, 29, 126−135

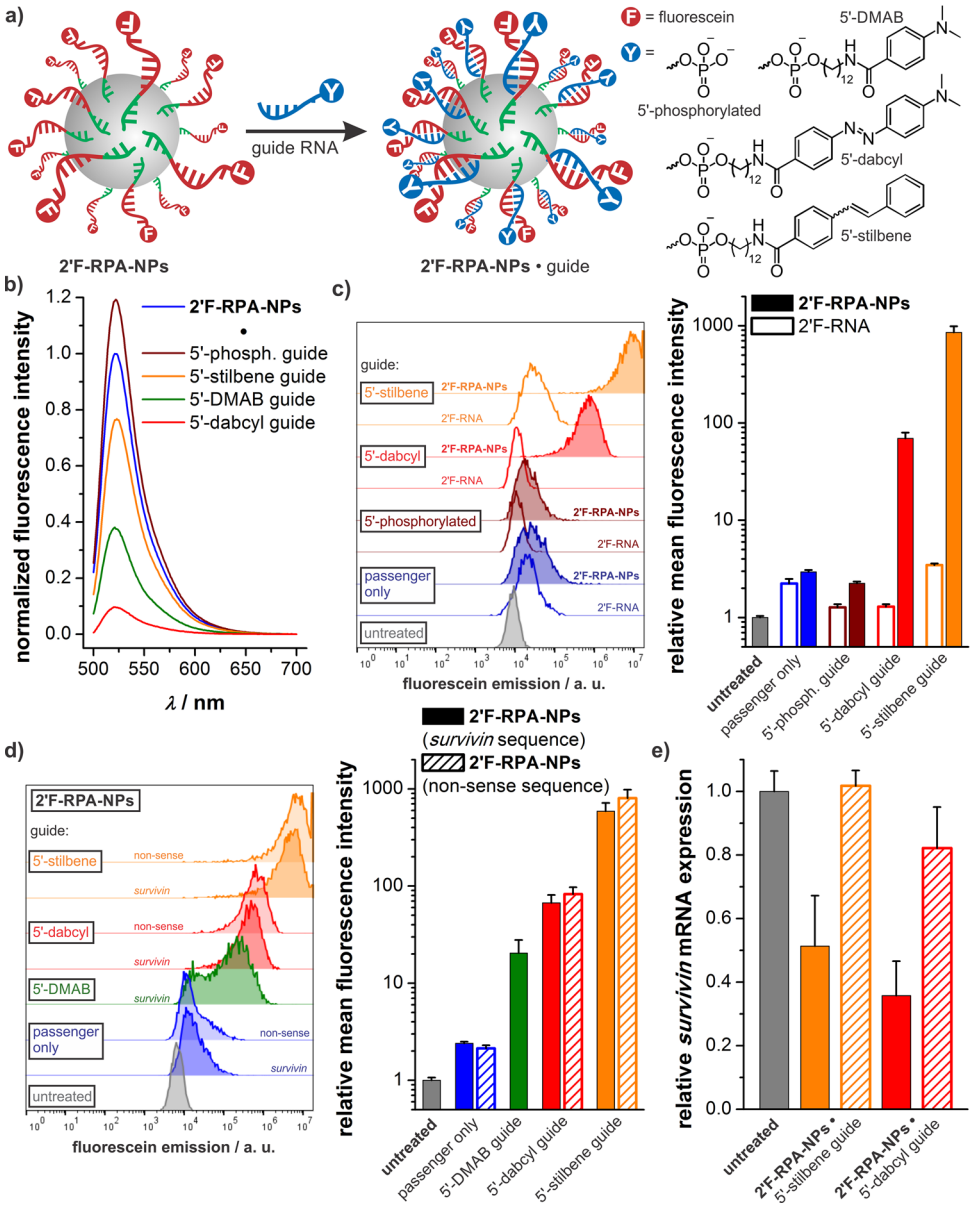

Figure 5. (a) **2′F-RPA-NPs** were hybridized with different chemically modified guide RNAs. (b) Fluorescence spectra of single- and double-stranded micelles. Each 5′-modification on the guide RNAs quenches the fluorescein dye on the micelle-displayed passenger strand to a different extent (200 nM passenger strand, 1.5 equiv guide strand in PBS, $\lambda_{ex.}$ = 485 nm, also see Figure S5e). Representative histograms and corresponding mean fluorescence intensities from flow cytometry measurements of HeLa cells treated with (c) *survivin* sequence-derived **2′F-RPA-NPs** or 2′F-RNAs and (d) *survivin* or nonsense sequence-derived **2′F-RPA-NPs** hybridized to different 5′-modified guide RNAs. (e) Relative *survivin* mRNA expression levels of HeLa cells treated with indicated *survivin* and nonsense sequence-derived micellar duplexes (single treatment with ca. 10 nM micelles in serum-free medium, analyzed after 50 h; see Supporting Information for detailed treatment protocols).

DISCUSSION

We identified two chemically similar structural motifs, dabcyl and stilbene, whose high-density display on micelle surfaces (in combination with a fluorescein dye) can trigger cell association and uptake of novel double-stranded RNA-polymer amphiphile nanoparticles. Other entities such as 4-*N*,*N*-dimethylamino-benzoic acid, phosphate, or hydroxide were significantly less competent or completely ineffective. Control experiments with free RNA duplexes revealed that the chemical moieties alone were not responsible for the effect. It was rather their high-density display on the outer corona of the spherical micelles that elicited uptake. We determined that the local effective concentration of the RNA that is displayed on the micelle surface lies in the range of 20−90 mM, which is 4−5 orders of magnitude higher than the overall (global) RNA concentration tested. It is conceivable that, once in contact with the outer cell membrane, the structural motifs displayed on the micelles are recognized by cell surface receptors involved in rather weak interactions. Because of their multivalent display at high local molarity this is still sufficient for effective binding and subsequent internalization. Contrarily, free RNAs bearing the same modifications would not remain bound long enough to be internalized, but soon diffuse away. In the future, it is important to investigate which genes are involved in the cellular uptake of micellar RNA and related nucleic acid-displaying nanomaterials. The identification of novel receptors responsible for uptake following such weak, but collective interactions governed by

DOI: 10.1021/acs.bioconjchem.7b00657
Bioconjugate Chem. 2018, 29, 126−135

multivalency might lead to the development of new ligands that can further modulate and enhance nanomaterial properties in a predictable or targeted fashion.

CONCLUSION

We introduced novel RNA-polymer amphiphiles that assemble into spherical micellar nanoparticles with diameters in the 15−30 nm range with narrow size distributions. **RPA-NPs** are soft organic quasi single-component structures that display RNA on their surface and can be reproducibly synthesized with little batch-to-batch and sequence-to-sequence variation. The incorporation of 2′-fluoropyrimidines protects the micellar RNA from degradation by serum nucleases. The RNA in the micelle corona remains accessible for hybridization with complementary RNA, which allows their formulation as biologically active double-stranded micellar siRNA. By modifying the 5′-terminus of the hybridized RNA we identified chemical moieties such as dabcyl and stilbene, that trigger the association with and uptake into HeLa cells without the need for toxic transfection reagents. The high density display of these modifications on the micelle shell was directly responsible for the observed increase in uptake efficiencies. The local RNA concentrations within the micelle corona was determined to be in the millimolar range. Thus, we speculate that weak interactions between the multivalently displayed structural motifs and cell surface receptors play a role. These interactions are not sufficiently strong enough to induce cell uptake of conventional, non-nanoparticulate RNAs that carry the same structural modifications. The micellar nanoparticles were capable of regulating intracellular *survivin* *m*RNA expression levels in a sequence-specific manner, while their knockdown potential was correlated to their uptake efficiencies. We believe that the high density display of small organic molecules that act as weak ligands for cell surface receptors provides a simple and straightforward way to modulate cell uptake properties of nucleic acid-derived micellar nanomaterials. The installation of such moieties can be readily achieved via hybridization of chemically modified complementary oligonucleotides into the micelle corona. Attachment of these modifiers can be achieved in a way that maintains biological functionality of the surface-displayed nucleic acids. Finally, it is conceivable that other classes of nanomaterials might also benefit from the high-density display of dabcyl- or stilbene-like structures in applications that call for cellular internalization.

EXPERIMENTAL PROCEDURES

General Remarks. Unless otherwise noted, all operations were performed at room temperature (RT). Oligonucleotide duplexes or double-stranded (**2′F**)**-RPA-NPs** were annealed prior to any experiment by heating buffered solutions for 5 min to 85−90 °C, followed by slow cooling to RT by switching off the heat block (ca. 1 h). All cell treatments were performed at 37 °C under 5% CO_2, except for handling.

Oligonucleotide and Polymer Synthesis. Oligonucleotides were assembled on a DNA/RNA synthesizer using commercially available phosphoramidite building blocks. Syntheses as well as cleavage/deprotection of oligonucleotide conjugates were carried out following standard procedures. Concentrations were determined via UV−vis spectroscopy and product identity and purity was verified by analytical HPLC and MALDI-TOF-MS. The synthesis of carboxy-terminated *poly*(-norbornyl) followed a previously published procedure,[31,33] and was characterized by SEC-MALS. See Supporting Information for details.

Conjugation of Carboxylic Acids to the 5′-Terminus of Amine-Modified Oligonculeotides on Solid Support. *Polymer Conjugation.* A solution of 10 equiv of carboxy-terminated poly(norbornyl) (50 mg, 10 μmol), 9 equiv HATU (3.4 mg, 9 μmol), and 30 equiv DIPEA (5.2 μL, 30 μmol) in 125 μL anhydrous DMF was preactivated for 10 min and subsequently added to the dried support bearing the 5′-amino-modified nucleic acid sequence (1 μmol with respect to the initial loading of the support). The synthesis column was shaken vigorously for 4−6 h, the support was washed with DMF and DCM and dried *in vacuo*. The coupling reaction was repeated once with fresh activated polymer overnight. The support was washed extensively with DMF and DCM to flush away unreacted polymer and dried *in vacuo*. Since only the full-length oligonucleotide bears a 5′-amino-modifier, each amphiphile resembles the correct full-length oligonucleotide sequence.

Conjugation with Small Molecules. A solution of 10 equiv of 4-((4-(dimethylamino)phenyl)azo)benzoic acid (dabcyl), 4-*N*,*N*-dimethylaminobenzoic acid (DMAB) or 4-stilbenecarboxylic acid, 9 equiv HATU, and 30 equiv DIPEA in anhydrous NMP was preactivated for 5 min and subsequently added to the dried support bearing the 5′-amino-modified nucleic acid sequence. The synthesis column was shaken for 2 h, the support was washed with NMP and DCM and dried *in vacuo*. The coupling reaction was repeated once with fresh activated carboxylic acid for 2 h. The support was washed extensively with NMP and DCM to flush away unreacted carboxylic acids and dried *in vacuo*.

Synthesis of RNA-Polymer Amphiphiles Nanoparticles (RPA-NPs). The support-bound, fully protected nucleic acid−polymer conjugate was immersed in 650 μL 30% ammonium hydroxide. After 1 h, 650 μL 40% aqueous methylamine was added and the support was incubated for 2 h at RT. The solution was removed and the support was washed twice with 2× 500 μL water and 2× 500 μL DMSO each. The combined solutions were dialyzed in 3500 M_W cutoff dialysis tubing against 2 L water (changed twice during 24 h) to remove the DMSO. The solution was reduced to ca. 1.5 mL by vacuum centrifugation. At this point, 250 μL DMSO was added and the solution was further reduced until the water was completely evaporated (a color switch of the fluorescein dye from bright yellow in aqueous solution to pale yellow in DMSO could be observed). To the resulting DMSO solution, 125 μL triethylamine hydrofluoride complex (NEt3 × 3 HF) was added, and the solution was incubated for 2.5 h at 65 °C to remove the 2′-TOM protecting groups. The reaction was quenched with 1.75 mL RNA quenching buffer and the solution was dialyzed in 3500 M_W cutoff dialysis tubing against 2 L water (changed twice during 24 h). Subsequently, the solution was filtered through 1.0 μm filters and reduced to 1 mL by vacuum centrifugation. An aliquot of this solution was kept for PAGE analysis ("crude"). Self-assembled micelles were purified from unconjugated nucleic acids via preparative size exclusion chromatography (SEC) and the fractions containing (**2′F**)**-RPA-NPs** were dialyzed in 10 000 M_W cutoff dialysis tubing against 2 L water (changed twice during 24 h) to remove salts from the elution buffer. The solution was further reduced to ca. 1 mL by vacuum centrifugation and finally filtered through 1.0 μm filters. The concentration of (**2′F**)-**RPA-NPs** was determined via UV−vis-spectroscopy. The

DOI: 10.1021/acs.bioconjchem.7b00657
Bioconjugate Chem. 2018, 29, 126−135

hydrodynamic diameter, morphology, and purity were determined via DLS, TEM (see Supporting Information for details), and PAGE, respectively.

UV−vis Spectroscopy. To determine concentrations of nucleic acid and **(2′F)-RPA-NP** stock solutions, aliquots were diluted with buffer (10 mM NaH_2PO_4, 100 mM NaCl, pH 7.0 for nucleic acids not labeled with fluorescein, 100 mM NaH_2PO_4, pH 9.0 for fluorescein-labeled nucleic acids and **(2′F)-RPA-NPs**). Measurements of the extinction E at 260 nm (for nucleic acids not labeled with fluorescein) or 495 nm (for fluorescein-labeled nucleic acids and **RPA-NPs**) yielded concentrations applying the Lambert−Beer Law ($E = \varepsilon \cdot c \cdot d$).

Melting Studies. Melting curves and associated melting temperatures (T_M) were measured by diluting nucleic acid conjugates and **(2′F)-RPA-NPs** in PBS to a final nucleic acid concentration of 1 μM each. The solutions were heated to 95 °C (10 °C·min^{-1}), equilibrated for 5 min, cooled to 25 °C (1 °C·min^{-1}) and equilibrated again for 5 min. Absorption at 260 nm was monitored three times during heating solutions from 25 to 95 °C (0.5 °C·min^{-1}). In the case of sigmoidal melting curves, first derivatives were calculated using the instrument software and the average of their maxima yielded the T_M.

Fluorescence Spectroscopy. Fluorescence spectra were recorded at oligonucleotide concentrations of 200 nM (fluorescein-labeled passenger strand) and 200 or 300 nM (complementary guide strands) in the denoted buffer. The excitation wavelength was set to 485 nm.

Polyacrylamide Gel Electrophoresis (PAGE). Gels contained 8 M urea (denaturing conditions) and consisted of a running gel layer (15% acrylamide) topped with a stacking gel layer (5% acrylamide). Samples were spiked with an equal volume of 2× TBE/Urea loading buffer, heated for 5 min to 85 °C, and cooled on ice before depositing into the gel pockets. Gel electrophoreses were performed in TBE-buffer at 200−250 V for ca. 45 min. Afterward, the fluorescein dye on oligonucleotides or **(2′F)-RPA-NPs** within the gel was imaged, before gels were stained with 25 mL of an aqueous ethidium bromide solution and imaged again.

RNase A Digestion Experiments. Fluorogenic substrates were added into PBS to give final concentrations of 200/300 nM (fluorescein-labeled passenger strand/dabcyl-labeled guide strand). Real-time kinetics were recorded in a plate reader, collecting time points in 60 s intervals. Excitation and emission wavelengths were set to 495 and 525 nm, respectively. Fluorescence was recorded for 10−12 min, the measurement was stopped, 1 μL of a 100× stock solution of RNase A in water was added to give final RNase A concentrations of 10−1000 pg·μL^{-1} and the measurement was continued for 120−150 min. The measurement was stopped, 1 μL of a 100× stock solution of RNase A was added to give a final RNase A concentration of 100 ng·μL^{-1}, and the measurement was continued until the fluorescence reached its maximum value. The data was normalized to the lowest and highest measured fluorescence intensities in each run. In the case of the duplex **2′F-RPA-NPs**·5′-dabcyl-2′F-guide, the data was normalized to the highest measured fluorescence intensity of the duplex **2′F-RPA-NPs**·5′-dabcyl-2′OH-guide.

Serum Stability. **(2′F)-RPA-NPs** were dissolved in PBS with or without 50 vol % human serum to a final concentration of 5 μM RNA. The solutions were incubated for 27 h at 37 °C and then for 70 h at RT, after which they were analyzed via PAGE.

Cell Uptake Studies. All cell treatments were performed in Opti-MEM reduced serum medium using three wells per treatment condition (96 well plate format) unless otherwise noted. To cells in 90 μL Opti-MEM, 10 μL of a 10× concentrated solution of single- or double-stranded oligonucleotides or **2′F-RPA-NPs** in PBS were added to the denoted final concentration. Cells were incubated for the denoted time and washed with 3× 100 μL DPBS prior to any measurement. After the third wash, 50 μL TrypLE was added to each well and cells were incubated for 10 min at 37 °C or until all cells have been detached from the plate bottom. Finally, 150 μL DPBS were added to each well and cells were analyzed immediately via flow cytometry (see Supporting Information for details).

Fluorescence Microscopy. HeLa cells were incubated in 90 μL Opti-MEM, to which 10 μL of a 10× concentrated solution of double-stranded micelles (**2′F-RPA-NPs** + 5′-dabcyl guide) in 1 × PBS were added (final concentration at treatment: 1 μM RNA). Cells were analyzed via fluorescence microscopy after 24 h.

Confocal Fluorescence Microscopy. HeLa cells were incubated in 270 μL Opti-MEM, to which 30 μL of a 10× concentrated solution of annealed double-stranded micelles (**2′F-RPA-NPs** + 5′-dabcyl guide) in 1 × PBS were added (final concentration at treatment: 1 μM RNA). After 5.5 h, cells were washed with 500 μL DPBS. For live cell imaging, CellMask Orange Plasma membrane stain (diluted 1:1000 in Opti-MEM, 200 μL) was added and cells were incubated for 10 min. The stain-containing medium was aspirated, and 200 μL Opti-MEM containing 1 μL Hoechst nucleus stain was added. Cells were imaged immediately. For fixed cell imaging, Wheat Germ Agglutinin Alexa Fluor 633 conjugate (diluted 1:100 in Opti-MEM, 200 μL) was added and cells were incubated for 10 min. The stain-containing medium was aspirated, and 100 μL of 3% paraformaldehyde in DPBS were added to fix the cells. After 10 min, the cells were washed with 2× 500 μL DPBS, and 1 drop of DAPI nucleus stain solution was added. Cells were kept at 12 °C and imaged within 24 h.

mRNA Regulation and Quantification. HeLa cells were incubated in 450 μL of the denoted medium, to which 50 μL of a 10× concentrated solution of single- or double-stranded micelles (**2′F-RPA-NPs**·guide RNA) in PBS were added to the denoted final concentration. After the denoted time, the medium was aspirated and cells were washed with 500 μL DPBS. *m*RNA extraction and quantification via RT-qPCR was performed as described in the Supporting Information.

■ ASSOCIATED CONTENT

Supporting Information

The Supporting Information is available free of charge on the ACS Publications website at DOI: 10.1021/acs.bioconjchem.7b00657.

Detailed descriptions of synthetic procedures, characterization of oligonucleotides and nanomaterials, and additional data and images (PDF)

■ AUTHOR INFORMATION

Corresponding Authors

*E-mail: geneyeo@ucsd.edu.

*E-mail: nathan.gianneschi@northwestern.edu.

ORCID

Nathan C. Gianneschi: 0000-0001-9945-5475

DOI: 10.1021/acs.bioconjchem.7b00657
Bioconjugate Chem. 2018, 29, 126−135

Notes

The authors declare no competing financial interest.

■ ACKNOWLEDGMENTS

This work was supported by grants from the National Science Foundation (DMR-1710105) to N.C.G and from the National Institutes of Health (HG004659, NS075449, HG007005) to G.W.Y. A.R. is the recipient of a fellowship within the Postdoc-Program of the German Academic Exchange Service (DAAD). We thank Dr. Joseph P. Patterson for performing TEM imaging on graphene oxide grids.

■ REFERENCES

(1) Meade, B. R., and Dowdy, S. F. (2009) The road to therapeutic RNA interference (RNAi): Tackling the 800 pound siRNA delivery gorilla. *Discovery Med. 8*, 253−6.
(2) Patil, S. D., Rhodes, D. G., and Burgess, D. J. (2005) DNA-based therapeutics and DNA delivery systems: A comprehensive review. *AAPS J. 7*, E61−E77.
(3) de Fougerolles, A., Vornlocher, H.-P., Maraganore, J., and Lieberman, J. (2007) Interfering with disease: a progress report on siRNA-based therapeutics. *Nat. Rev. Drug Discovery 6*, 443−53.
(4) Kim, D. H., and Rossi, J. J. (2007) Strategies for silencing human disease using RNA interference. *Nat. Rev. Genet. 8*, 173−84.
(5) Famulok, M., Hartig, J. S., and Mayer, G. (2007) Functional Aptamers and Aptazymes in Biotechnology, Diagnostics, and Therapy. *Chem. Rev. 107*, 3715−3743.
(6) Doudna, J. A., and Cech, T. R. (2002) The chemical repertoire of natural ribozymes. *Nature 418*, 222−228.
(7) He, L., and Hannon, G. J. (2004) MicroRNAs: Small RNAs with a big role in gene regulation. *Nat. Rev. Genet. 5*, 522−531.
(8) Elbashir, S. M., Harborth, J., Lendeckel, W., Yalcin, A., Weber, K., and Tuschl, T. (2001) Duplexes of 21-nucleotide RNAs mediate RNA interference in cultured mammalian cells. *Nature 411*, 494−498.
(9) Kwon, I., and Schaffer, D. (2008) Designer Gene Delivery Vectors: Molecular Engineering and Evolution of Adeno-Associated Viral Vectors for Enhanced Gene Transfer. *Pharm. Res. 25*, 489−499.
(10) Marshall, E. (1999) Clinical trials - Gene therapy death prompts review of adenovirus vector. *Science 286*, 2244−2245.
(11) Davis, M. E. (2002) Non-viral gene delivery systems. *Curr. Opin. Biotechnol. 13*, 128−131.
(12) Thomas, M., and Klibanov, A. M. (2003) Non-viral gene therapy: polycation-mediated DNA delivery. *Appl. Microbiol. Biotechnol. 62*, 27−34.
(13) Semple, S. C., Akinc, A., Chen, J., Sandhu, A. P., Mui, B. L., Cho, C. K., Sah, D. W. Y., Stebbing, D., Crosley, E. J., Yaworski, E., Hafez, I. M., Dorkin, J. R., Qin, J., Lam, K., Rajeev, K. G., Wong, K. F., Jeffs, L. B., Nechev, L., Eisenhardt, M. L., Jayaraman, M., Kazem, M., Maier, M. A., Srinivasulu, M., Weinstein, M. J., Chen, Q., Alvarez, R., Barros, S. A., De, S., Klimuk, S. K., Borland, T., Kosovrasti, V., Cantley, W. L., Tam, Y. K., Manoharan, M., Ciufolini, M. A., Tracy, M. A., de Fougerolles, A., MacLachlan, I., Cullis, P. R., Madden, T. D., and Hope, M. J. (2010) Rational design of cationic lipids for siRNA delivery. *Nat. Biotechnol. 28*, 172−176.
(14) Wei, H., Volpatti, L. R., Sellers, D. L., Maris, D. O., Andrews, I. W., Hemphill, A. S., Chan, L. W., Chu, D. S. H., Horner, P. J., and Pun, S. H. (2013) Dual Responsive, Stabilized Nanoparticles for Efficient In Vivo Plasmid Delivery. *Angew. Chem., Int. Ed. 52*, 5377−5381.
(15) Johnson, M. E., Shon, J., Guan, B. M., Patterson, J. P., Oldenhuis, N. J., Eldredge, A. C., Gianneschi, N. C., and Guan, Z. (2016) Fluorocarbon Modified Low-Molecular-Weight Polyethylenimine for siRNA Delivery. *Bioconjugate Chem. 27*, 1784−1788.
(16) Lv, H., Zhang, S., Wang, B., Cui, S., and Yan, J. (2006) Toxicity of cationic lipids and cationic polymers in gene delivery. *J. Controlled Release 114*, 100−109.
(17) Guo, P. (2010) The emerging field of RNA nanotechnology. *Nat. Nanotechnol. 5*, 833−42.
(18) Dunn, S. S., Tian, S., Blake, S., Wang, J., Galloway, A. L., Murphy, A., Pohlhaus, P. D., Rolland, J. P., Napier, M. E., and DeSimone, J. M. (2012) Reductively responsive siRNA-conjugated hydrogel nanoparticles for gene silencing. *J. Am. Chem. Soc. 134*, 7423−30.
(19) Shu, Y., Pi, F., Sharma, A., Rajabi, M., Haque, F., Shu, D., Leggas, M., Evers, B. M., and and Guo, P. (2014) Stable RNA nanoparticles as potential new generation drugs for cancer therapy. *Adv. Drug Delivery Rev. 66*, 74−89.
(20) Giljohann, D. A., Seferos, D. S., Prigodich, A. E., Patel, P. C., and Mirkin, C. A. (2009) Gene regulation with polyvalent siRNA-nanoparticle conjugates. *J. Am. Chem. Soc. 131*, 2072−3.
(21) Rouge, J. L., Hao, L., Wu, X. a, Briley, W. E., and Mirkin, C. A. (2014) Spherical Nucleic Acids as a Divergent Platform for Synthesizing RNA−Nanoparticle Conjugates through Enzymatic Ligation. *ACS Nano 8*, 8837−8843.
(22) Barnaby, S. N., Lee, A., and Mirkin, C. A. (2014) Probing the inherent stability of siRNA immobilized on nanoparticle constructs. *Proc. Natl. Acad. Sci. U. S. A. 111*, 9739−9744.
(23) Chinen, A. B., Ferrer, J. R., Merkel, T. J., and Mirkin, C. A. (2016) Relationships between Poly(ethylene glycol) Modifications on RNA−Spherical Nucleic Acid Conjugates and Cellular Uptake and Circulation Time. *Bioconjugate Chem. 27*, 2715−2721.
(24) Zheng, D., Giljohann, D. A., Chen, D. L., Massich, M. D., Wang, X.-Q., Iordanov, H., Mirkin, C. A., and Paller, A. S. (2012) Topical delivery of siRNA-based spherical nucleic acid nanoparticle conjugates for gene regulation. *Proc. Natl. Acad. Sci. U. S. A. 109*, 11975−11980.
(25) Jensen, S. A., Day, E. S., Ko, C. H., Hurley, L. A., Luciano, J. P., Kouri, F. M., Merkel, T. J., Luthi, A. J., Patel, P. C., Cutler, J. I., Daniel, W. L., Scott, A. W., Rotz, M. W., Meade, T. J., Giljohann, D. A., Mirkin, C. A., and Stegh, A. H. (2013) Spherical nucleic acid nanoparticle conjugates as an RNAi-based therapy for glioblastoma. *Sci. Transl. Med. 5*, 209ra152.
(26) Alkilany, A. M., and Murphy, C. J. (2010) Toxicity and cellular uptake of gold nanoparticles: what we have learned so far? *J. Nanopart. Res. 12*, 2313−2333.
(27) Wu, X. A., Choi, C. H. J., Zhang, C., Hao, L., and Mirkin, C. A. (2014) Intracellular Fate of Spherical Nucleic Acid Nanoparticle Conjugates. *J. Am. Chem. Soc. 136*, 7726−7733.
(28) Chompoosor, A., Saha, K., Ghosh, P. S., Macarthy, D. J., Miranda, O. R., Zhu, Z.-J., Arcaro, K. F., and Rotello, V. M. (2010) The Role of Surface Functionality on Acute Cytotoxicity, ROS Generation and DNA Damage by Cationic Gold Nanoparticles. *Small 6*, 2246−2249.
(29) Chien, M.-P., Rush, A. M., Thompson, M. P., and Gianneschi, N. C. (2010) Programmable Shape-Shifting Micelles. *Angew. Chem., Int. Ed. 49*, 5076−5080.
(30) Chien, M.-P., Thompson, M. P., and Gianneschi, N. C. (2011) DNA-nanoparticle micelles as supramolecular fluorogenic substrates enabling catalytic signal amplification and detection by DNAzyme probes. *Chem. Commun. 47*, 167−9.
(31) Rush, A. M., Thompson, M. P., Tatro, E. T., and Gianneschi, N. C. (2013) Nuclease-Resistant DNA via High-Density Packing in Polymeric Micellar Nanoparticle Coronas. *ACS Nano 7*, 1379−1387.
(32) Roloff, A., Carlini, A. S., Callmann, C. E., and Gianneschi, N. C. (2017) Micellar Thrombin-Binding Aptamers: Reversible Nanoscale Anticoagulants. *J. Am. Chem. Soc. 139*, 16442.
(33) Rush, A. M., Nelles, D. A., Blum, A. P., Barnhill, S. A., Tatro, E. T., Yeo, G. W., and Gianneschi, N. C. (2014) Intracellular mRNA Regulation with Self-Assembled Locked Nucleic Acid Polymer Nanoparticles. *J. Am. Chem. Soc. 136*, 7615−7618.
(34) Kappler, M., Köhler, T., Kampf, C., Diestelkötter, P., Würl, P., Schmitz, M., Bartel, F., Lautenschläger, C., Rieber, E. P., Schmidt, H., Bache, M., Taubert, H., and Meye, A. (2001) Increased survivin transcript levels: An independent negative predictor of survival in soft tissue sarcoma patients. *Int. J. Cancer 95*, 360−363.
(35) Kappler, M., Bache, M., Bartel, F., Kotzsch, M., Panian, M., Würl, P., Blümke, K., Schmidt, H., Meye, A., and Taubert, H. (2004) Knockdown of survivin expression by small interfering RNA reduces

DOI: 10.1021/acs.bioconjchem.7b00657
Bioconjugate Chem. 2018, 29, 126−135

the clonogenic survival of human sarcoma cell lines independently of p53. *Cancer Gene Ther. 11*, 186−193.
(36) Paduano, F., Villa, R., Pennati, M., Folini, M., Binda, M., Daidone, M. G., and Zaffaroni, N. (2006) Silencing of survivin gene by small interfering RNAs produces supra-additive growth suppression in combination with 17-allylamino-17-demethoxygeldanamycin in human prostate cancer cells. *Mol. Cancer Ther. 5*, 179−86.
(37) Lytton-Jean, A. K. R., and Mirkin, C. A. (2005) A thermodynamic investigation into the binding properties of DNA functionalized gold nanoparticle probes and molecular fluorophore probes. *J. Am. Chem. Soc. 127*, 12754−5.
(38) Barnhill, S. A., Bell, N. C., Patterson, J. P., Olds, D. P., and Gianneschi, N. C. (2015) Phase Diagrams of Polynorbornene Amphiphilic Block Copolymers in Solution. *Macromolecules 48*, 1152−1161.
(39) Kim, J. H., Estabrook, R. A., Braun, G., Lee, B. R., and Reich, N. O. (2007) Specific and sensitive detection of nucleic acids and RNases using gold nanoparticle-RNA-fluorescent dye conjugates. *Chem. Commun.*, 4342−4.
(40) Barnaby, S. N., Thaner, R. V., Ross, M. B., Brown, K. A., Schatz, G. C., and Mirkin, C. A. (2015) Modular and Chemically Responsive Oligonucleotide "Bonds" in Nanoparticle Superlattices. *J. Am. Chem. Soc. 137*, 13566−13571.
(41) Pieken, W. A., Olsen, D. B., Benseler, F., Aurup, H., and Eckstein, F. (1991) Kinetic Characterization of Ribonuclease-Resistant 2′-Modified Hammerhead Ribozymes. *Science 253*, 314−317.
(42) Chiu, Y.-L., and Rana, T. M. (2003) siRNA function in RNAi: A chemical modification analysis. *RNA 9*, 1034−1048.
(43) Manoharan, M., Akinc, A., Pandey, R. K., Qin, J., Hadwiger, P., John, M., Mills, K., Charisse, K., Maier, M. A., Nechev, L., Greene, E. M., Pallan, P. S., Rozners, E., Rajeev, K. G., and Egli, M. (2011) Unique Gene-Silencing and Structural Properties of 2′-Fluoro-Modified siRNAs. *Angew. Chem., Int. Ed. 50*, 2284−2288.
(44) Martinez, J., Patkaniowska, A., Urlaub, H., Lührmann, R., and Tuschl, T. (2002) Single-stranded antisense siRNAs guide target RNA cleavage in RNAi. *Cell 110*, 563−574.
(45) Tan, X., Li, B. B., Lu, X., Jia, F., Santori, C., Menon, P., Li, H., Zhang, B., Zhao, J. J., and Zhang, K. (2015) Light-Triggered, Self-Immolative Nucleic Acid-Drug Nanostructures. *J. Am. Chem. Soc. 137*, 6112−6115.
(46) Raines, R. T. (1998) Ribonuclease A. *Chem. Rev. 98*, 1045−1065.
(47) Park, C., and Raines, R. T. (2003) Catalysis by Ribonuclease A Is Limited by the Rate of Substrate Association. *Biochemistry 42*, 3509−3518.
(48) Schwarz, D. S., Hutvágner, G., Haley, B., and Zamore, P. D. (2002) Evidence that siRNAs function as guides, not primers, in the Drosophila and human RNAi pathways. *Mol. Cell 10*, 537−548.
(49) Harborth, J., Elbashir, S. M., Vandenburgh, K., Manninga, H., Scaringe, S. A., Weber, K., and Tuschl, T. (2003) Sequence, Chemical, and Structural Variation of Small Interfering RNAs and Short Hairpin RNAs and the Effect on Mammalian Gene Silencing. *Antisense Nucleic Acid Drug Dev. 13*, 83−105.
(50) Manoharan, M. (2004) RNA interference and chemically modified small interfering RNAs. *Curr. Opin. Chem. Biol. 8*, 570−579.
(51) Arraiano, C. M., Mauxion, F., Viegas, S. C., Matos, R. G., and Séraphin, B. (2013) Intracellular ribonucleases involved in transcript processing and decay: Precision tools for RNA. *Biochim. Biophys. Acta, Gene Regul. Mech. 1829*, 491−513.

DOI: 10.1021/acs.bioconjchem.7b00657
Bioconjugate Chem. 2018, 29, 126−135